Plug and Thermal Barrier Potential Formation in Gamma 10

I. Katanuma

Plasma Research Center

Univ. Tsukuba, Japan

Introduction

Tandem mirror Gamma 10 employs thermal barrier to insulate the electrons in the end plugs from those in the central cell. Generation of thermal barrier in Gamma 10 requires the creation of a hot mirror trapped electron population, heated by electron cyclotron resonance heating. We calculate the creation of hot electron population when only second harmonic electron cyclotron resonance heating is included in the thermal barrier region. We also calculate the plug and thermal barrier potential formation when fundamental electron heating and neutral beam injections are added, by using our bounce averaged Fokker-Planck code.

Hot Electron Build Up

To study the hot electron build up at thermal barrier region theoretically and numerically, we include the quasilinear electron heating effects in Fokker-Planck equation,

$$\frac{\partial f}{\partial t} = \left(\frac{\partial f}{\partial t}\right)_c + \frac{1}{v_\perp}\frac{\partial}{\partial v_\perp}\left(v_\perp D \frac{\partial f}{\partial v_\perp}\right) \quad ,$$

$$D = \pi \left(\frac{e}{2m_e\omega}\right)^2 \sum_\ell \ell^2\omega^2_{ce} \left|E^+\right|^2 \delta(\omega - \ell\omega_{ce}) \, J^2_{\ell-1}\left(\frac{k_\perp v_\perp}{\omega_{ce}}\right) \quad , \tag{1}$$

$$E^+ \equiv E_x + iE_y \quad .$$

Here we use standard notation and E^+ is ECRH electric field, $J_{\ell-1}$ is Bessel function, $k_\perp$ is perpendicular mode number, ω is wave frequency. The first term in right hand side of Eq. (1) is Fokker-Planck collision term. We assume $k_\parallel = 0$ and $E_\parallel = 0$ for simplicity. At first by using Eq. (1) we calculate the hot electron build up when only second harmonic resonance heating effects are included and its resonance point exists at the midplane in a mirror cell. Bounce averaging Eq. (1) along particle orbit, we have at resonance point,

$$\frac{\partial f}{\partial t} = \frac{1}{v_\perp}\frac{\partial}{\partial v_\perp}\left(v_\perp \langle D\rangle \frac{\partial f}{\partial v_\perp}\right) \quad ,$$

$$\langle D\rangle = \int_{orbit} D \frac{dz}{v_\parallel} \Big/ \int_{orbit} \frac{dz}{v_\parallel}$$

$$= 2\pi \left(\frac{e}{2m_e}\right)^2 \frac{1}{\omega} \left|E^+\right|^2 J_0^{\,2} \Big/ \left(v_\parallel \tau_B \frac{1}{B}\frac{dB}{dZ}\right) \quad , \tag{2}$$

$$\tau_B = \int_{orbit} \frac{d\ell}{v_\parallel} \quad .$$

We have a equation for hot electron build up by integrating Eq. (2) multiplied by $\frac{1}{2} m_e v_\perp^{\,2}$.

$$\frac{\partial}{\partial t} n_h T_{h\perp} = n_h T_{h\perp} / \tau_b$$

$$\tau_b^{-1} = 4\pi \left(\frac{e}{2m_e}\right)^2 |E^+|^2 \frac{1}{\omega c^2} N_\perp^2 / \left(v_\parallel \tau_B \frac{1}{B} \frac{dB}{dZ}\right) \tag{3}$$

$$N_\perp = k_\perp C / \omega \quad .$$

Here we consider only quasilinear term of Eq. (1). For the thermal barrier region of Gamma 10 we have τ_b numerically,

$$\tau_b = 2.36 \times 10^{-6} \frac{\omega}{\omega_{ce}(10_{kgauss})} / \left(\left|\frac{E^+(v/cm)}{100}\right|^2 N_\perp^2\right) \text{ sec.} \tag{4}$$

For $|E^+| = 100$v/cm, $N_\perp = 1$, $\omega/\omega_{ce} = 1$, we have $\tau_b \simeq 2.36\mu$sec. This build up time is so fast, then quasi-steady state will be realized. In this quasi-steady state hot electron pitch angle scattering will contribute the further evolution of hot electron density in the thermal barrier region. So we consider hot electron pitch angle scattering effects. In this quasi-steady state, the following equation will hold,

$$\frac{1}{v_\perp} \frac{\partial}{\partial v_\perp} \left(v_\perp \langle D \rangle \frac{\partial f_h}{\partial v_\perp}\right) = 0 \quad , \tag{5}$$

on $v_\parallel = 0$ line at the midplane. One solution of Eq. (5) is

$$f_h(v) = \frac{n_h}{2\pi v_{max}} v_\perp^{-2} \delta(v_\parallel) \quad , \tag{6}$$

here v_{max} is the maximum velocity of hot electrons, above which electrons are not heated by ECRH due to the relativistic electron mass shifts. Then we assume the electron distribution function to collide with hot electrons in quasi-steady state as

$$f(v,\theta) = \frac{n_c}{\pi^{3/2} v_e^{\,3}} \exp\left(-\frac{v^2}{v_e^{\,2}}\right) + \frac{n_h}{2\pi v_{max}} v^{-2}\delta(\theta-\pi/2) \quad , \tag{7}$$

$$v_e^{\,2} = 2\,T_c/m_e$$

In this case linearlized Fokker-Planck equation becomes

$$\frac{\partial f_n}{\partial t} = n_c \left\{\frac{1}{v^2}\frac{\partial}{\partial v}\left(f_h + \frac{v_e^{\,2}}{2v}\frac{\partial f_h}{\partial v}\right) + \frac{1}{2v^3}\frac{\partial}{\partial \mu}\left[(1-\mu^2)\frac{\partial f_h}{\partial \mu}\right]\right\}\Gamma$$

$$+ n_h \left\{\frac{2}{v_{max}} v^{-2}\delta(\theta-\pi/2) f_h + \frac{1}{2v^2 v_{max}} \ell n \left|\frac{v+v_{max}}{v}\right| \frac{\partial^2 f_h}{\partial \theta^2}\right. \tag{8}$$

$$\left. + \frac{1}{2v v_{max}}\left[\ell n \left|\frac{v+v_{max}}{v}\right| + \frac{v_{max}}{v}\right]\frac{\partial f_h}{\partial v}\right\}\Gamma \quad .$$

Here $\Gamma = \frac{4\pi e^{+}\ell n\Lambda}{m_e^{\,2}}$, $\mu = \cos\theta$. We estimate $\frac{\partial^2 f_h}{\partial \theta^2} = -\frac{f_h}{(\Delta\theta)^2}$. Integrating Eq. (8) for (v, θ), we have

$$\frac{\partial n_h}{\partial t} = -\left(\frac{1}{\tau_{cd}} + \frac{1}{\tau_{cs}} + \frac{1}{\tau_{hd}} + \frac{1}{\tau_{hs}}\right) n_h \quad .$$

Here

$$\tau_{hs} = 4\tau_D \frac{n_c}{n_h} (\Delta\theta)^2 \left(\frac{E_{max}}{T_e}\right)\left(\frac{E_{min}}{T_e}\right)^{1/2} / \ell n\,(E_{max}/E_{min}) \quad ,$$

$$\tau_{cs} = 4\tau_D (\Delta\theta)^2 \left(\frac{E_{max}}{T_e}\right)^{1/2}\left(\frac{E_{min}}{T_e}\right) \quad ,$$

$$\tau_{hd} = 2\tau_D \frac{n_c}{n_h} \left(\frac{E_{max}}{T_e}\right)^{1/2} \left(\frac{E_{min}}{T_e}\right) \quad ,$$

$$\tau_{cd} = \tau_D \left(\frac{E_{max}}{T_e}\right)^{1/2} \left(\frac{E_{min}}{T_e}\right) \quad ,$$

$$\tau_D = \frac{\sqrt{m_e}\, T_e^{3/2}}{\sqrt{2}\pi n_c e^4 \ell n \Lambda} \quad ,$$

$$E_{max} = \frac{1}{2} m_e v_{max}^2 \quad ,$$

$$E_{min} = \frac{1}{2} m_e v_{min}^2 \quad ,$$

$$n_h = \int_{v_{min}}^{v_{max}} 2\pi v^2 dv \int_0^{\Delta\theta} \sin\theta \, d\theta f_h \quad .$$

τ_{hs}, τ_{cs}, τ_{cd}, and τ_{hd} are the escaping time of hot electrons out of the resonance region in the velocity space by hot-hot electron pitch angle scattering, hot-cold electron pitch angle scattering, hot-cold electron drag, hot-hot electron drag, respectively. Pitch angle scattering makes the hot electrons loss from the ECRH resonance region and so contribute to the hot electron density build up in the thermal barrier region. Electron drag reduces the hot electron density. For the parameters of $n_c = 10^{12}$/cc, $n_h = 5 \times 10^{11}$/cc, $T_e = 100$eV, $E_{max} = 50$ keV, $E_{min} = 2$ keV, $\Delta\theta = 10^\circ$, we have $\tau_{hs} = 2.9$msec, $\tau_{hd} = 30$msec, $\tau_{cs} = 0.93$msec, $\tau_{cd} = 7.8$msec. Then for this parameters hot-cold electron pitch angle scattering is the dominant process for the hot electron density build up, and its build up time is of order of 1 msec.

Simulation results

First we show the results of the case of second harmonic electron resonance heating in the thermal barrier region of Gamma 10. The parameters used are $T_i = T_e = 100$ eV, $n_i = n_e = 10^{12}$/cc at mirror throat. Figure 1 shows the systematic diagram of Gamma 10 and magnetic field profile used in the simulation. Figure 2 shows the bounce averaged Fokker-Planck coefficient for

the case of $|E^+|$ = 100 v/cm. You can see the heating region is localized around $v_{\parallel}$ = 0 line. Figure 3 is also Fokker-Planck coefficient which is the amplitude of $v_{\parallel}$ = 0 line in Fig. 2. This coefficient is proportional to energy E and in the region $E \gtrsim 50$ keV this coefficient becomes small due to relativistic electron mass shift. Figure 4 is the time evolution of potential, hot electron density and energy at the midplane. Hot electron internal energy T_h builds up at early time and saturated after that time. Hot electron density also builds up at early time, but does not saturate and builds up further more with a slow growth rate after that time. From Figure 4 in first build up phase the hot electrons are heated directly by ECRH and then its density and internal energy grows. In the second build up phase hot electron pitch angle scattering is a dominant process so hot electron density builds up even through its internal energy has saturated as is predicted by theoretical consideration. Electrostatic potential becomes negative in first build up phase because electrons flow in the mirror trapped region from the passing region by ECRH, while ion density is not afffected by ECRH. In the second build up pahse, however, electrostatic potential grows in the positive direction. This shows that the collisional filling rate is larger than that of hot electron density built up by ECRH. At 3 msec the final steady state is realized in the simulation. We show the steady state potential, density, hot electron density and energy profiles along the magnetic field in Fig. 5. Remarkable feature is that electrostatic potential is negative compared with that at the mirror throat even though any ion pumping is not included in this simulation. However, this potential dip is not sufficient for the thermal barrier because passing electron energy from the throat is 100 eV while this potential dip is only -26 V. Density has its maximum value at the midplane which shows there are many ions trapped in the potential well around the midplane. Hoe electrons are localized around the midplane. There are about 36% hot electrons at the midplane. Figure 6 is the steady state electron

distribution function on $v_{\parallel} = 0$ line as a function of electron energy E. This distribution function is proportional to E^{-1} in the high energy region even in the steady state.

Next we show the results of the case in which the ion pumping is included. Pumping is added for the Fokker-Planck equation of ions. Simulation parameters are the same as the previous simulation and ion pumping time ν^{-1} is 200 μsec. Figure 7 is the steady state electron and ion distribution function. Ions are pumped and then the ions in the mirror trapped region are modified strongly from Maxwellian. Figure 8 is the potential and density profile along the magentic field. Because of ion pumping, the density is smaller at the midplane than that of the mirror throat. In the case potential is -343 V at the midplane which is large enough for the thermal barrier. Next we show the results of neutral beam injection. The parameters used are $|E^{+}| = 100$ V/cm at midplane and $|E^{+}| = 100$ V/cm at plug region. Neutral beam density $n_b = 3 \times 10^{10}$/cc, background neutral $n_0 = 3 \times 10^{9}$/cc, ion and electron passing density and temperature are 10^{12}/cc and 100 eV, respectively. Neutral beam injection angle and energy are 41° and 25 keV, respectively. Neutral beam and background neutral are hydrogen atom. Figure 9 is the results of the simulation in the steady state. There is no thermal barrier at the midplane. Figure 10 is also the results of the simulation in the steady state. However, in this case the charge exchange and ionization between neutral beam and sloshing hot ions are omitted artificially. In this case there is a thermal barrier at the midplane even though the potential dip is not so large. You can see a plug potential at the plug region which is sufficient for plugging the passing ions.

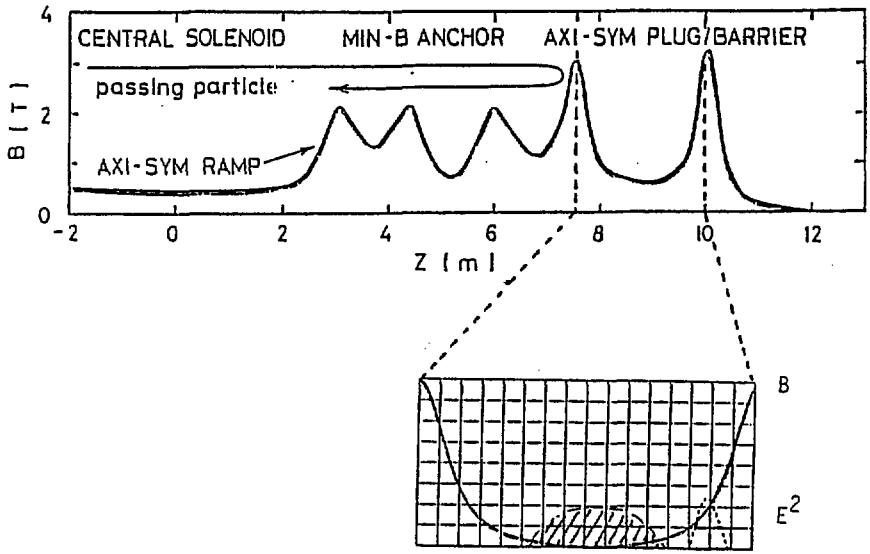

Fig. 1

$$\frac{\partial f}{\partial t} = C_{vv} \frac{\partial^2 f}{\partial v^2} + \cdots$$

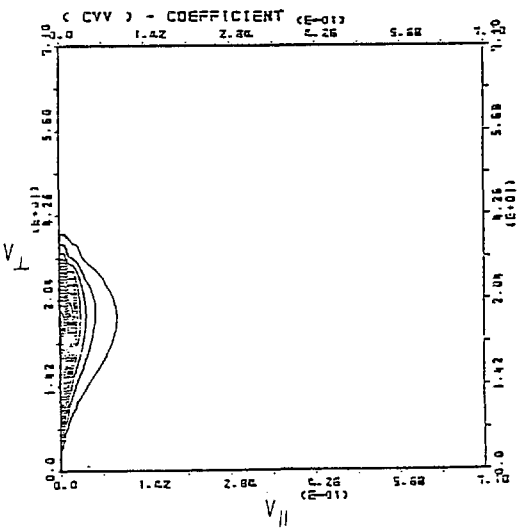

Fig. 2

$$\frac{\partial f}{\partial t} = C_{vv} \frac{\partial^2 f}{\partial v^2} + \cdots$$

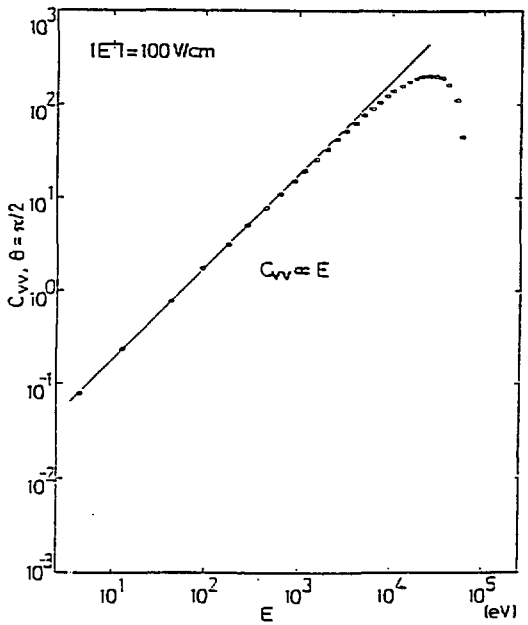

Fig. 3

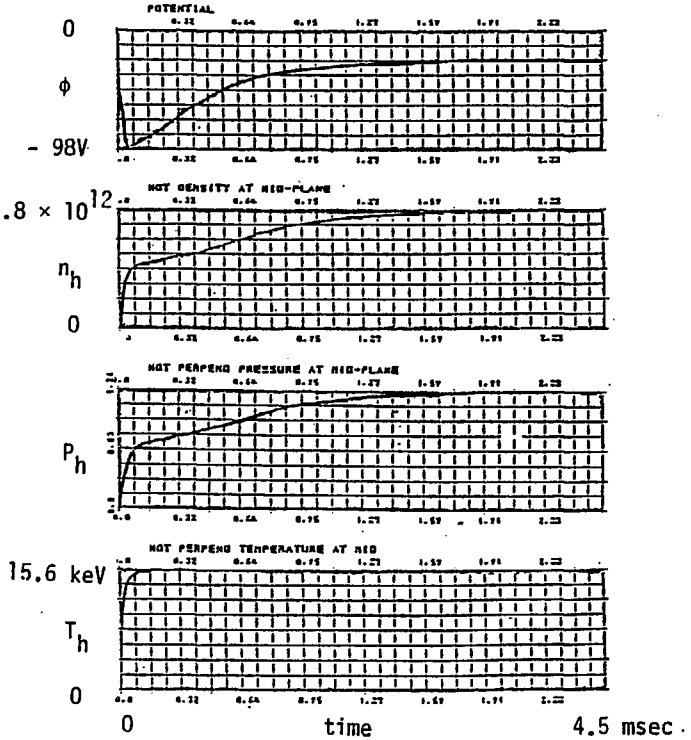

Fig. 4

steady state

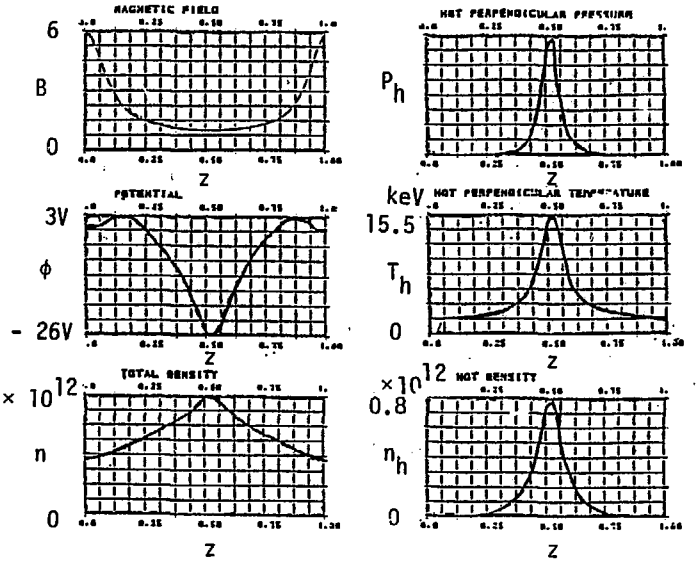

Fig. 5

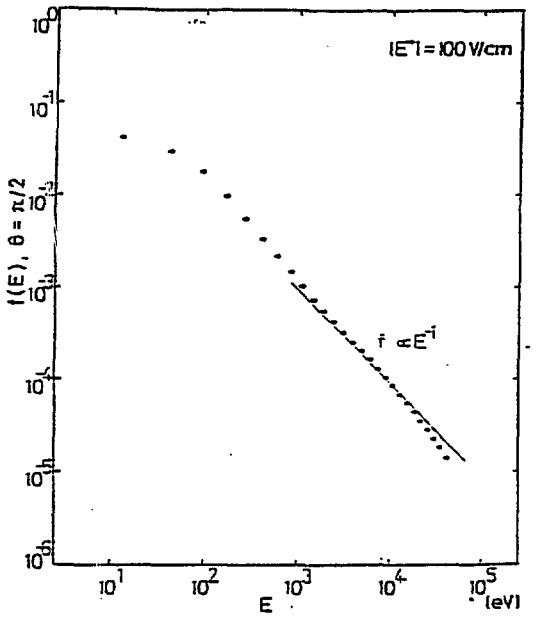

Fig. 6

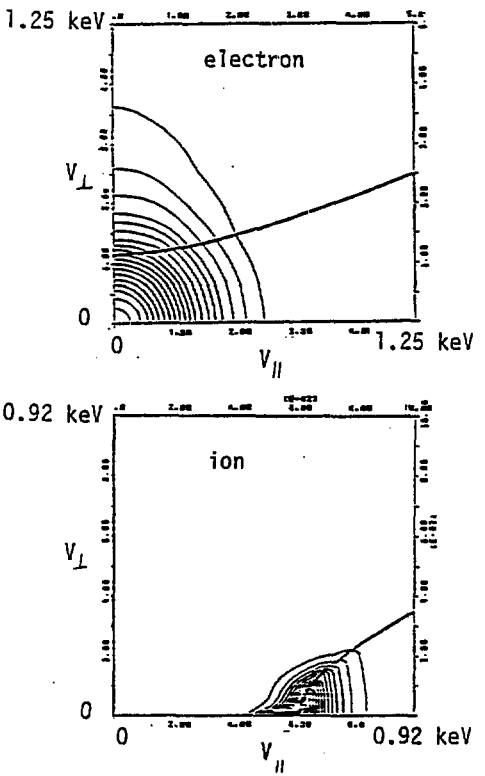

Fig. 7

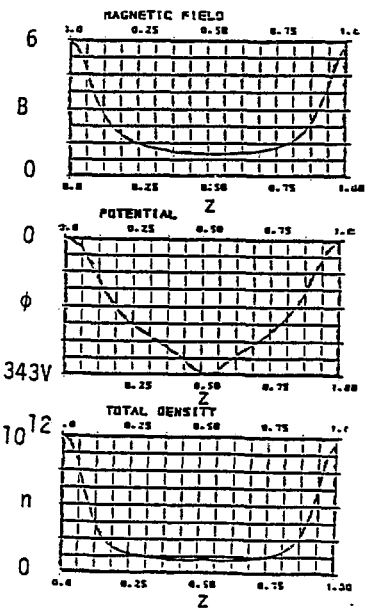

Fig. 8

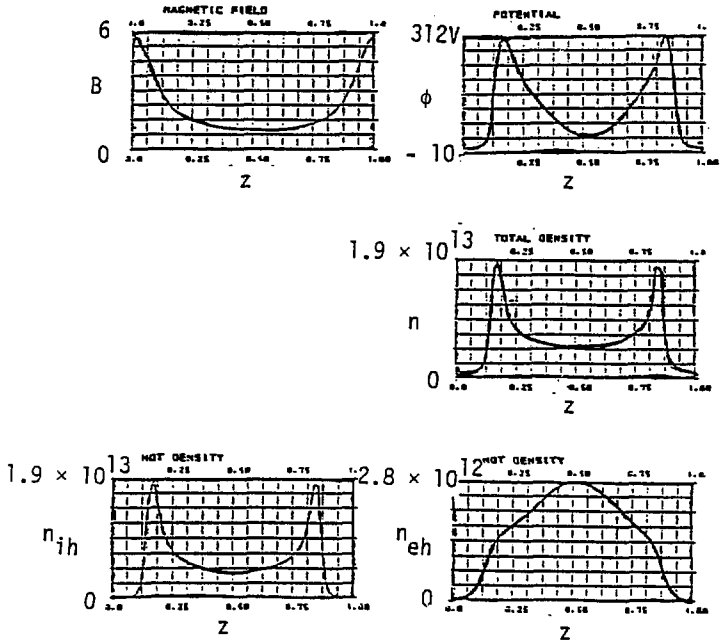
MAGNETIC FIELD
6
B
0
Z
POTENTIAL
312V
ϕ
- 10
Z
1.9 × 10^13
TOTAL DENSITY
n
0
Z
1.9 × 10^13
HOT DENSITY
n_ih
0
Z
2.8 × 10^12
HOT DENSITY
n_eh
0
Z

Fig. 9

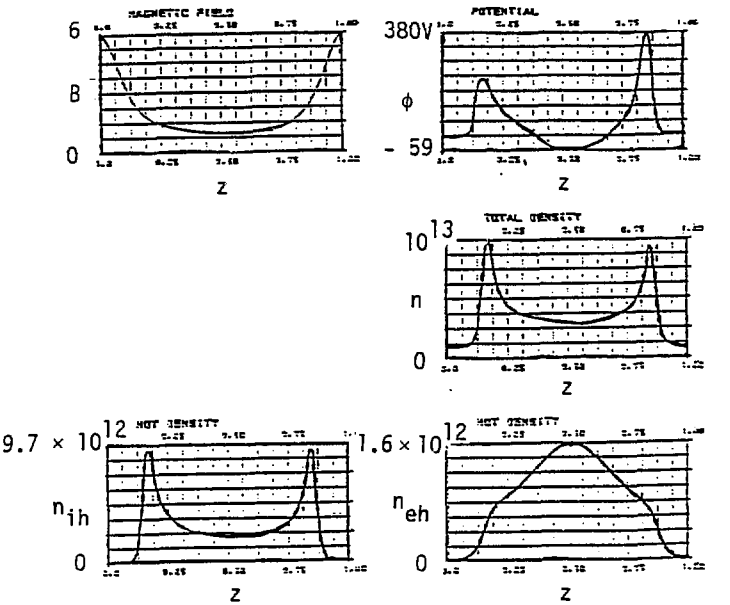
MAGNETIC FIELD
6
B
0
Z
POTENTIAL
380V
ϕ
- 59
Z
10^13
TOTAL DENSITY
n
0
Z
9.7 × 10^12
HOT DENSITY
n_ih
0
Z
1.6 × 10^12
HOT DENSITY
n_eh
0
Z

Fig. 10